

Research Article

A far-infrared search for planet nine using AKARI all-sky survey

Amos Y.A. Chen¹, Tomotsugu Goto^{1,2}, Issei Yamamura³, Takao Nakagawa^{3,4}, Cossas K.-W. Wu², Terry Long Phan², Tetsuya Hashimoto⁵, Yuri Uno⁵, Simon C.-C. Ho^{6,7,8,9} and Seong Jin Kim²

¹Department of Physics, National Tsing Hua University, Hsinchu, Taiwan, ²Institute of Astronomy, National Tsing Hua University, Hsinchu, Taiwan, ³Institute of Space and Astronautical Science, Japan Aerospace Exploration Agency, Sagami-hara, Kanagawa, Japan, ⁴Advanced Research Laboratories, Tokyo City University, Setagaya-ku, Tokyo, Japan, ⁵Department of Physics, National Chung Hsing University, Taichung, Taiwan, ⁶Research School of Astronomy and Astrophysics, The Australian National University, Canberra, ACT, Australia, ⁷Centre for Astrophysics and Supercomputing, Swinburne University of Technology, Hawthorn, VIC, Australia, ⁸OzGrav: The Australian Research Council Centre of Excellence for Gravitational Wave Discovery, Hawthorn, VIC, Australia and ⁹ASTRO3D: ARC Centre of Excellence for All-sky Astrophysics in 3D, Canberra, ACT, Australia

Abstract

An unusual orbital element clustering of Kuiper belt objects (KBOs) has been observed. The most promising dynamic solution is the presence of a giant planet in the outer Solar system, Planet Nine. However, due to its extreme distance, intensive searches in optical have not been successful. We aim to find Planet Nine in the far-infrared, where it has the peak of the black body radiation, using the most sensitive all-sky far-infrared survey to date, *AKARI*. In contrast to optical searches, where the energy of reflected sunlight decreases by d^4 , thermal radiation in the infrared decreases with the square of the heliocentric distance d^2 . We search for moving objects in the *AKARI* Single Scan Detection List. We select sources from a promising region suggested by an N-body simulation from Millholland and Laughlin 2017: $30^\circ < \text{R.A.} < 50^\circ$ and $-20^\circ < \text{Dec.} < 20^\circ$. Known sources are excluded by cross-matching *AKARI* sources with 9 optical and infrared catalogues. Furthermore, we select sources with small background strength to avoid sources in the cirrus. Since Planet Nine is stationary in a timescale of hours but moves on a monthly scale, our primary strategy is to select slowly moving objects that are stationary in 24 h but not in six months, using multiple single scans by *AKARI*. The selected slowly moving *AKARI* sources are scrutinised for potential contamination from cosmic rays. Our analysis reveals two possible Planet Nine candidates whose positions and flux are within the theoretical prediction ranges. These candidates warrant further investigation through follow-up observations to confirm the existence and properties of Planet Nine.

Keywords: Infrared: general; methods: data analysis; planets and satellites: detection

(Received 10 January 2025; revised 12 April 2025; accepted 2 May 2025)

1. Introduction

The unexpected clustering of a set of distant Kuiper Belt Objects (KBOs) claimed by Batygin & Brown (2016) suggests the presence of a massive object in the outer Solar system. This object could be an unknown planet – called Planet Nine – or even a primordial black hole (Scholtz & Unwin 2020). Numerous studies support the hypothesis of Planet Nine to account for this phenomenon. Batygin & Brown (2016) employed an n-body simulation to model the impact of a perturber on the orbits of test particles. They showed that the observed KBOs with such clustering of the argument of perihelion are only 0.007% likely to occur by chance, and their simulations suggested that the existence of Planet Nine could produce this clustering.

However, there are several studies arguing that the clustering of extreme trans-Neptune Objects (TNOs) arises from the observational bias. Shankman et al. (2017) reported a uniform distribution of eight extreme TNOs discovered by the Outer Solar System Origins Survey (OSSOS; Bannister et al. 2016) survey.

Bernardinelli et al. (2020) found no significant clustering of seven extreme TNOs from the Dark Energy Survey (DES; The Dark Energy Survey Collaboration 2005). Napier et al. (2021) examined 14 extreme TNOs reported in the OSSOS, DES, and Sheppard & Trujillo (2016) studies, concluding that the mean scaled longitude of perihelion and orbital poles of the identified extreme TNOs align with a uniformly distributed population at a range between 17% and 94%. Although Napier et al. (2021) showed no clustering of TNOs, their work did not rule out the Planet Nine hypothesis due to the limited observation area.

In light of these competing interpretations, a recent paper Batygin et al. (2024) presented a new simulation on the orbits of long-period TNOs. They correct for observational biases and compare their N-body simulation result with the perihelion distribution of 17 long-period TNOs from the Minor Planet Center database. Their result showed that the perihelion distribution of these TNOs rejects the scenario without Planet Nine at the $\sim 5\text{-}\sigma$ confidence level. Several simulation papers have also provided predictions regarding the characteristics of Planet Nine. Batygin & Brown (2016) estimated that Planet Nine is on a 700 au semimajor axis and 0.6 eccentricity orbit with 10 Earth masses (M_\oplus). Their updated simulation with a more complete setup (Brown & Batygin 2019) suggested Planet Nine is on an orbit with semimajor axis 380^{+140}_{-80} au and perihelion distance 300^{+85}_{-60} au with

Corresponding author: Amos Y.A. Chen, Email: yuanchen@gapp.nthu.edu.tw.

Cite this article: Chen A, Goto T, Yamamura I, Nakagawa T, Wu C, Phan TL, Hashimoto T, Uno Y, Ho S and Kim SJ. (2025) A far-infrared search for planet nine using *AKARI* all-sky survey. *Publications of the Astronomical Society of Australia* 42, e061, 1–10. <https://doi.org/10.1017/pasa.2025.10037>

$6.2^{+2.2}_{-1.3} M_{\oplus}$. Another simulation work (Millholland & Laughlin 2017, hereafter ML17) focused on the mean motion resonances between known KBOs and Planet Nine. They suggested that Planet Nine is on an orbit with a semimajor axis of 654 au and eccentricity of 0.45, separated 400–900 au from Earth and 6 to 12 M_{\oplus} .

There were various works that searched for Planet Nine. Some previous studies expected to detect reflected Sunlight from Planet Nine in optical wide-field surveys, e.g., Zwicky Transient Facility (ZTF) (Brown & Batygin 2022), Dark Energy Survey (DES) (Belyakov, Bernardinelli, & Brown 2022), and Pan-STARRS1 (Brown, Holman, & Batygin 2024). Other searches utilised near-infrared all-sky surveys such as the Wide-field Infrared Survey Explorer (WISE) (Fotney et al. 2016) and NEOWISE (Meisner et al. 2017), but those searches were not successful. Naess et al. (2021) analysed millimetre-wave data from the Atacama Cosmology Telescope (ACT) and provided 10 possible Planet Nine candidates.

In this work, we try to find the thermal radiation of Planet Nine from the *AKARI* far-infrared all-sky survey data. The benefit of searching in far-infrared wavelengths is that the intensity of radiation does not drop as quickly as reflected light. Reflected Sunlight will decrease by d^4 as the distance d increases, while thermal radiation falls by d^2 . Cowan, Holder, & Kaib (2016) suggested that current and planned microwave detectors would detect Planet Nine. Other pioneering works searched for thermal radiation from Planet Nine in far-infrared all-sky surveys (e.g. Rowan-Robinson 2021; Sedgwick & Serjeant 2022). Rowan-Robinson (2021) searched in InfraRed Astronomical Satellite (IRAS) data and found one candidate with estimated distance 225 ± 15 au and $3\text{--}5 M_{\oplus}$, which is not consistent with most of the predictions. Sedgwick & Serjeant (2022) searched for moving objects that have detections in the IRAS catalogues and *AKARI*-FIS Bright Source Catalogue (FISBSC). They found 535 potential candidates after spectral energy distribution (SED) fits. Since all of them are located in the cirrus cloud, there is no good Planet Nine candidate.

Planet Nine was estimated to have a temperature range between 53 and 28 K (Cowan, Holder, & Kaib 2016), corresponding to black body radiation peaks at 54.7 and 103.5 μm . *AKARI* Far Infrared Surveyor (FIS) instrument was equipped with four filters spanning 50–180 μm (Kawada et al. 2007), which is ideal for searching for thermal emission in this temperature range. In this study, we use a dedicated source list “*AKARI*-FIS Single Scan Detection List (hereafter FISSSDL; see Section 2). Fig. 1 shows the histogram of the FISSSDL sources (log N – log S plot), where S in Jy is the source flux, and N is the number of objects at the flux. The most sensitive band, WIDE-S, has a peak at ~ 0.2 Jy, lower than FISBSC Version 2 (~ 0.44 Jy) and IRAS Faint Source Catalogue (~ 1.0 Jy at 100 μm), and includes even fainter sources. Although most of them are possibly fake sources caused by cosmic rays, there is a chance of detecting Planet Nine candidates if we carefully examine the list. Rowan-Robinson (2021), Sedgwick & Serjeant (2022) required detection in IRAS, which limited the survey to > 1.0 Jy in 100 μm . Only requiring *AKARI* detection can expand the search to five times fainter objects.

The paper is structured as follows. We describe the data in Section 2. Selection details in Section 3. Results in Section 4. Discussion and conclusion in Section 5.

2. *AKARI*-FIS single scan detection list

The infrared astronomical satellite *AKARI* (Murakami et al. 2007) was equipped with a 68.5 cm aperture cooled telescope and two

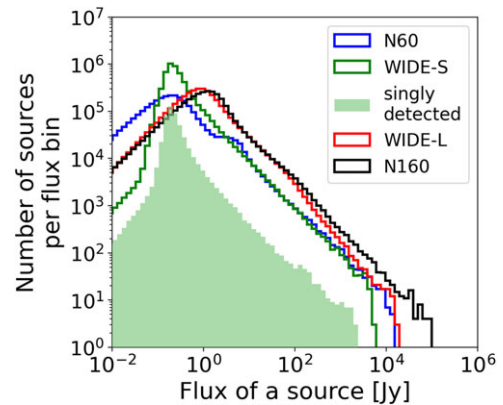


Figure 1. Flux histograms of FISSSDL sources. Four histograms correspond to four *AKARI*/FIS filters. The bin size is on a logarithmic scale, totalling 80 bins. Sources detected in the N60 filter (centred at 65 μm) are represented in blue, those detected by the WIDE-S filter (90 μm) are in green, the WIDE-L filter (140 μm) results are shown in red, and the N160 filter (160 μm) sources are depicted in black. The green shaded histogram shows the sources that were only detected once by the *AKARI*/WIDE-S.

science instruments: Far-Infrared Surveyor (FIS; Kawada et al. 2007) and Infrared Camera (IRC; Onaka et al. 2007). *AKARI* was launched in 2006 and carried out the All-Sky Survey in four far-infrared wavelength bands and two mid-infrared wavelength bands as well as thousands of pointed observations of particular targets or sky areas from May 2006 to August 2007. After cryogen (liquid helium) depletion, *AKARI* continued observation until February 2011, only in the near-infrared wavelengths.

Infrared point source catalogues were produced from the all-sky survey data. The *AKARI*-FIS Bright Source Catalogue (FISBSC; Yamamura et al. 2010) includes 411 (Version 1) and 501 (Version 2) thousand sources observed in four wavelengths centred at 65, 90, 140 and 160 μm . FISBSC has already been used to search for Planet Nine (Sedgwick & Serjeant 2022).

However, the FISBSC is not optimal for our search for Planet Nine because moving objects can be removed from the catalogue. *AKARI* scanned a position of the sky in a few to several successive orbits, then revisited the position after half a year. The number of scans depends on the Ecliptic latitude and the survey operation program, ranging from zero to several hundred. In the construction of FISBSC, a condition is set to confirm whether a signal is from a real, stationary source that it is detected in at least two scans and at least 3/4 of the total number of scans observed at the position. This condition rejects moving targets and includes Planet Nine. Therefore, we created a dedicated source list, FISSSDL, for the Planet Nine search, from the same intermediate data used for FISBSC. FISSSDL relaxes the above confirmation condition and includes any source that was detected at least once. This change of the confirmation policy allows moving objects such as Planet Nine to be included, with the risk of contamination by many fake signals, such as cosmic rays (CRs) hits and instrumental artefacts. We carried out a careful investigation to find Planet Nine candidates, as we explain in the following sections.

3. Methods

To select Planet Nine from *AKARI* FISSSDL, it is important to make sure that Planet Nine is bright enough to be detected by *AKARI*. Fig. 1 shows a histogram of all FISSSDL sources detected in 4 filters. The *AKARI*/WIDE-S (90 μm) filter has a lower

peak value compared to AKARI/WIDE-L and AKARI/N160. AKARI/WIDE-S detects more sources than the AKARI/N60 filter. We confirm that the WIDE-S filter is the most sensitive AKARI/FIS filter.

Therefore, we focus on the 90 μm flux of the sources in this work. Estimation of flux and motion of Planet Nine is described in Sections 3.1 and 3.2. In Section 3.3, based on the simulation results (ML17), we select candidates from the most promising area; Section 3.4: exclude known sources by cross-match with known catalogues; Section 3.5: exclude sources potentially contaminated by cirrus; Section 3.6: exclude non-moving sources; Section 3.7: exclude contamination from CRs and select candidates with clear detection.

3.1 Flux estimation

To calculate the flux from Planet Nine, we need to know the radius of Planet Nine. Previous simulation works (e.g. Batygin & Brown 2016; Brown & Batygin 2019; Brown & Batygin 2019; Millholland & Laughlin 2017) predicted the mass of Planet Nine and its orbital parameters, but there is no implication of Planet Nine's average density. Here, we assume that Planet Nine has an average density of Neptune and Uranus $\rho = (\rho_{\text{Neptune}} + \rho_{\text{Uranus}})/2 = 1.454\text{g/cm}^3$. The size of Planet Nine can then be derived from the mass and average density. The estimated effective temperature of Planet Nine ranges from 28 to 53 K, with energy mainly from internal heat (Cowan, Holder, & Kaib 2016). The expected flux of black body radiation from Planet Nine at 90 μm can be calculated as a function of distance d and mass M of Planet Nine:

$$F = SR \frac{\Omega \lambda^2}{c} \quad (1)$$

$$\Omega = \frac{\pi R^2}{d^2} = \frac{\pi}{d^2} \left(\frac{3M}{4\pi\rho} \right)^{2/3} \quad (2)$$

F is flux in Jansky, SR is the spectral radiance in unit $[W/m^3/sr]$, Ω is the solid angle in unit $[sr]$, c is the speed of light and wavelength λ is 90 μm . The radius of Planet Nine R can be calculated from M and density ρ . We adopt the mass range of 6–12 M_{\oplus} predicted by ML17. We derive the black body's spectral radiance at 90 μm for temperatures of 28 and 53 K suggested by Cowan, Holder, & Kaib (2016); then, we plug in Eq. (1) to calculate the expected flux from Planet Nine. We use the mass range from ML17 to maintain consistency in this work. We adopt the promising area from ML17, so we also use the mass range predicted by ML17. We use the Planet Nine parameters estimated by ML17 rather than Brown & Batygin (2019) because 78% of the parameter space predicted by Brown & Batygin (2019) is ruled out by recent surveys (Brown & Batygin 2022; Belyakov, Bernardinelli, & Brown 2022; Brown, Holman, & Batygin 2024). Brown, Holman, & Batygin (2024) combined three surveys and excluded orbits with Planet Nine brighter than 21 V magnitude, which roughly corresponds to 500 au. However, the constraints on larger distances remain weak. On the other hand, ML17 predicted a Planet Nine orbit with a more significant distance (~ 800 au), which has not yet been fully investigated.

The expected flux of Planet Nine with different parameters is plotted in the left panel of Fig. 2. The right panel of Fig. 2 shows the histogram of 90 μm flux (FLUX90) of FISSSDL sources, and those sources that passed through flux selection are comparable to Planet Nine's expected flux at 53 K. Brown & Batygin (2019) used Wu & Lithwick (2013)'s mass-radius relation derived from the

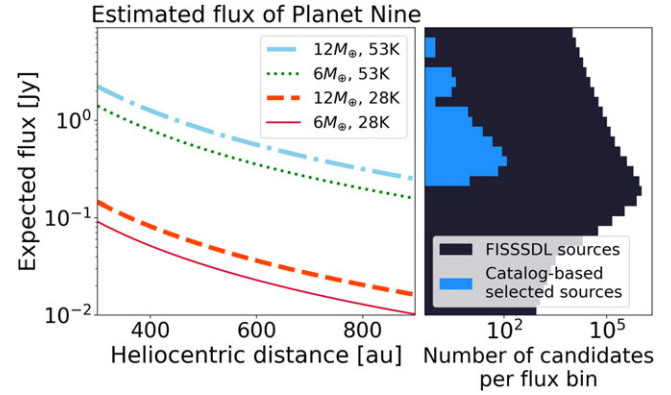


Figure 2. Left: Estimated 90 μm flux of Planet Nine. We calculate the expected Planet Nine's 90 μm flux in Section 3.1 and plot it with 4 combinations of 2 parameters: mass and temperature in the left panel. The x-axis is the heliocentric distance of Planet Nine. The mass range of 6–12 M_{\oplus} was predicted by ML17. Cowan, Holder, & Kaib (2016) suggested a temperature range of 28–53 K. Right: A histogram of FLUX90. The dark blue histogram shows the flux distribution of FISSSDL sources with the same y-axis as the left panel. 393 candidates selected from FISSSDL after cross-matching with known catalogues (Section 3.4), FLUX90/FERR90 > 3 and BG90 < 0.2 in catalogue unit (Section 3.5), and no monthly confirmation (Section 3.5) is shown in the light blue histogram. The X-axis shows the number of sources in each bin. The bin size is the same as Fig. 1.

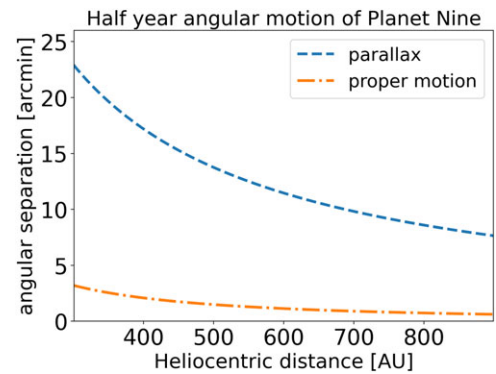


Figure 3. Anticipated proper motion and parallax of Planet Nine within half a year. The overall angular displacement is the vector sum of the proper motion and the parallax. In the time scale of half a year, parallax dominates the angular motion, so we only consider the parallax of Planet Nine in this work.

Kepler planets, $M \simeq 3M_{\oplus}(R/R_{\oplus})$, to estimate the radius of Planet Nine. If we adopt their mass-radius relation, the expected spectral flux drops by 50% at 6 M_{\oplus} and increases by 30% at the 12 M_{\oplus} situation, which is comparable with a constant density assumption within our interest mass range.

3.2 Expected motion

The angular motion of Planet Nine is composed of proper motion and parallax, which can be calculated by equations 4 and 7 in (Cowan, Holder, & Kaib 2016). Their value as a function of distance to Earth is shown in Fig. 3. Planet Nine's parallax over six months ranges from 10 to 25 arcmin, depending on its distance to the Earth. The proper motion ranges from 0.6 to 3.2 arcmin, which is much smaller than parallax. Therefore, we only consider the parallax of Planet Nine in this work. The astrometric accuracy of the AKARI FISBSC is 3.5'', so the parallax is detectable by AKARI with observations spaced six months apart, but not within a single

Table 1. Catalogues used for cross-matching with AKARI FISSSDL. All data we used for cross-matching were accessed from the CDS cross-matching service.

Catalog name	Number of sources	Filters	Reference	Cross-match radius (")
MASS	470 992 970	J, H, K	Skrutskie et al. (2006)	7.1
NOMAD	1 117 612 732	B, V, R, J, H, and K	Zacharias et al. (2004)	5.3
PS1	1 919 106 885	g, r, i, z, and y	Chambers et al. (2016)	4.5
WISE	563 921 584	3.4, 4.6, 12, and 22 μm	Wright et al. (2010)	7.9
ALLWISE	747 634 026	3.4, 4.6, 12, and 22 μm	Mainzer et al. (2011)	8.0
unWISE	2 214 734 224	3.4, 4.6, 12, and 22 μm	Schlafly, Meisner, & Green (2019)	4.9
CatWISE2020	1 890 715 640	3.4, 4.6, 12, and 22 μm	Schlafly, Meisner, & Green (2021)	5.1
SIMBAD	17 959 486	B,V,R,J,H,K,u,g,r,i, and z	Wenger et al. (2000)	3.7
SDSS DR16	1 231 051 050	u,g,r,i, and z	Ahumada et al. (2020)	4.9
AKARI FISSSDL	5 274 338	65, 90, 140, and 160 μm		

day. The one-hour parallax of Planet Nine at 300 au is only $0.23''$. Therefore, we look for stationary objects in hours time scale, but moving in months time scale as good candidates for Planet Nine.

3.3 Position selection

The dynamical simulation from ML17 suggests that the probability of finding Planet Nine is higher in the region $30^\circ < \text{R.A.} < 50^\circ$, $-20^\circ < \text{Dec.} < 20^\circ$. This region also overlaps with the area suggested by Brown & Batygin (2019). There are 50 033 sources in this area out of 5 274 338 sources in FISSSDL.

3.4 Cross-match with 9 catalogues

Some stationary objects or known Solar-system objects can be included in the FISSSDL. To exclude known sources, we cross-match AKARI FISSSDL with 9 external catalogues: 2MASS, NOMAD, Pan-STARRS DR1(PS1), WISE, ALLWISE, CatWISE2020, unWISE, SIMBAD, and SDSS DR16. Their properties are described in Table 1. Because these observations are carried out in different years, if an object is found in multiple catalogues at the same position, it is not a moving object and thus not Planet Nine.

The cross-matching of AKARI FISSSDL with the other 9 catalogues listed in Table 1 aims to exclude stable sources. However, due to spurious sources in the FISSSDL, there are randomly matched pairs in the cross-matching result. To model the distribution of random sources and avoid the effect from the galactic plane, we generate 20 000 random sources with a uniform distribution across the region galactic latitude (b) $b > 10^\circ$ and cross-match with 9 target catalogues. We cross-match $b > 10^\circ$ FISSSDL sources with those 9 catalogues and find the separation distribution of real and randomly matched sources. Sources that are at least $32''$ apart are considered distinct by definition in the point source catalogue processing (Yamamura et al. 2010). Thus, randomly matched pairs should dominate the separation distribution larger than $32''$. We fit the FISSSDL cross-match distribution at separations larger than $32''$ with the distribution of random pairs and find the portion of randomly matched sources (see Fig. 4). After subtracting the contribution from the randomly matched pairs, we are able to fit the separation distribution of the real matched pairs with the Gaussian distribution. The Gaussian fitting results are shown in the last column of Table 1. The $1-\sigma$ radius from this Gaussian fit is taken as the cross-match radius for the respective catalogue.

Suppose the distance between an AKARI source and its corresponding source in a catalogue is less than the cross-match radius specific to that catalogue; we consider them to be the same object and remove this AKARI source. After this process, 29 901 sources remain.

To exclude possible IRAS sources included in AKARI FISSSDL, we try to apply a similar analysis to IRAS's catalogues. However, due to the small number of sources in IRAS catalogues (245 889 sources in the IRAS Point Source Catalog (PSC) and 173 044 sources in the IRAS Faint Source Catalog (FSC), which is 3 to 4 orders less than other catalogues listed in Table 1), we are not able to fit the separation distribution of matched FISSSDL IRAS sources with the random pairs at $32'' < \text{separation} < 120''$. Thus, despite the similarity of IRAS and AKARI, we do not cross-match between FISSSDL and IRAS's catalogues. We use the positional uncertainty from IRAS PSC and IRAS FSC, and only 53 out of 29 901 sources are matched. The effect of not cross-matching with IRAS is very minor, and those candidates are also excluded in the flux selection step.

3.5 Flux selection

To ensure reliable flux measurements unaffected by the cirrus effect, we utilise the index of background strength at 90 μm (BG90, in arbitrary unit)^a from the AKARI FISSSDL to identify candidates. In the FLUX90-BG90 plot Fig. 5, the number of sources peaks at BG90 = 0.3, and we find that most of these sources come from the cirrus region in our target area. To remove sources contaminated by cirrus, we select sources with BG90 < 0.2 ($\sim 4 \text{ MJy/SR}$). We also require flux over flux error (FERR90) larger than 5 at 90 μm (FLUX90/FERR90 > 5) to select sources with reliable flux. In this step, 1 726 sources out of 29 901 sources are selected.

3.6. Detection selection

Based on the discussion in Section 3.2, AKARI should be able to detect six months' parallax motion of Planet Nine if it is located from 300 to 900 au. The FISBSC, as well as FISSSDL, contain

^aWe use the face values in the catalogue, where the unit is not specified yet because the background values are not calibrated.

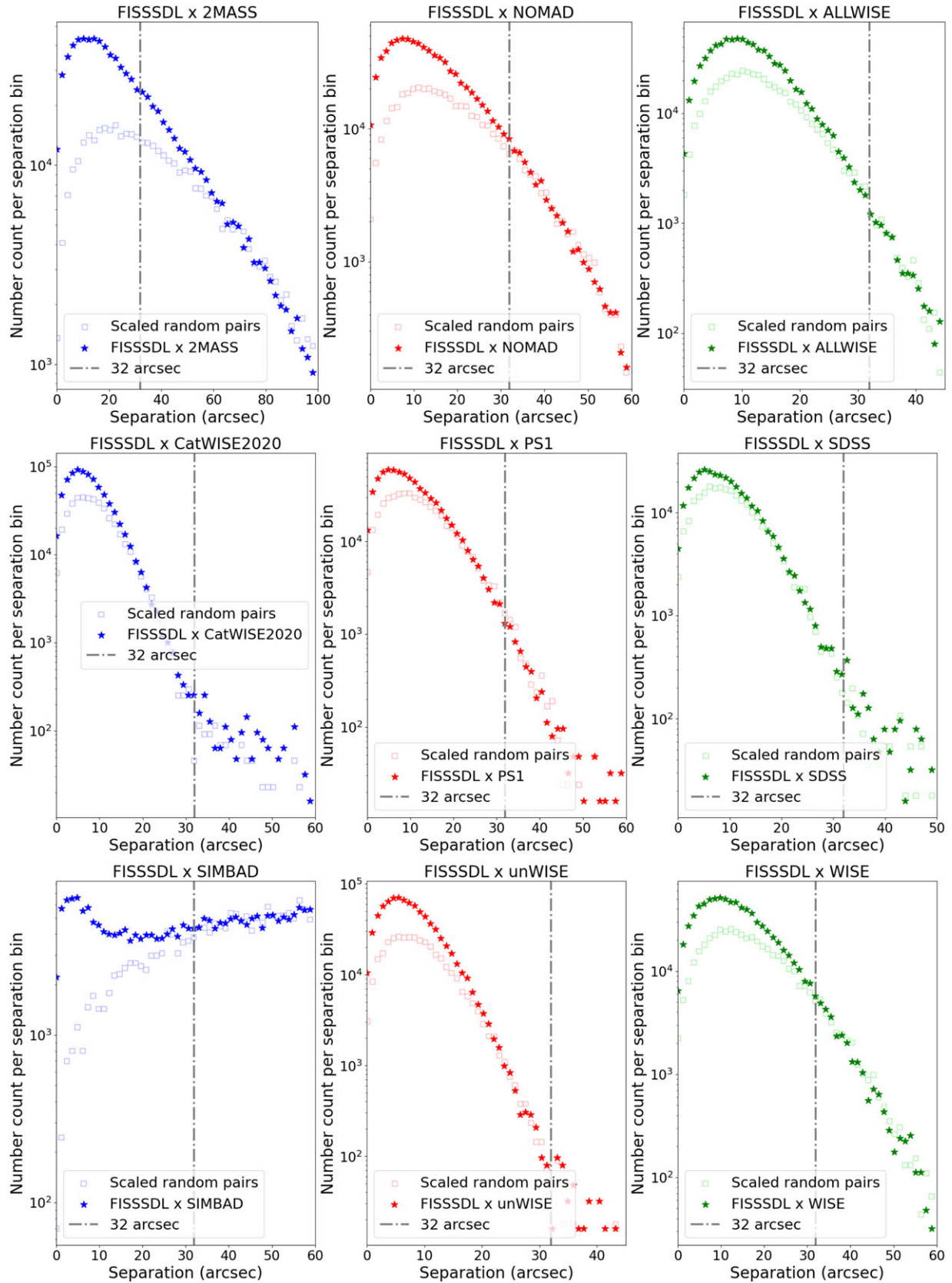


Figure 4. Separation distribution of matched sources. There are 50 bins on a linear scale in each subplot. The stars show the separation of matched pairs of *AKARI* sources and sources from catalogues in Table 1. Squares represent the scaled separation between matched random sources and sources from the corresponding catalogue. The vertical dash line represents 32", beyond which two sources are treated as distinct. (see Section 3.4).

Table 2. List of two Planet Nine candidates and their 90 μm fluxes of each detection. POSERRMJ and POSERRMI are major and minor axes of position error. POSERRPA is the position angle. The epoch of the coordinate system is J2000.

Name	Flux 1 (Jy)	Flux 2 (Jy)	R.A. (deg)	Dec. (deg)	POSERRMJ (arcsec)	POSERRMI (arcsec)	POSERRPA (deg)	Detected Epoch
FISSSDL J0250422-150114	0.61	1.62	42.676	−15.021	3.5	2.3	340.3	2007/07/28
FISSSDL J0301112-164240	1.27	0.51	45.297	−16.711	3.5	2.3	340.7	2006/07/30

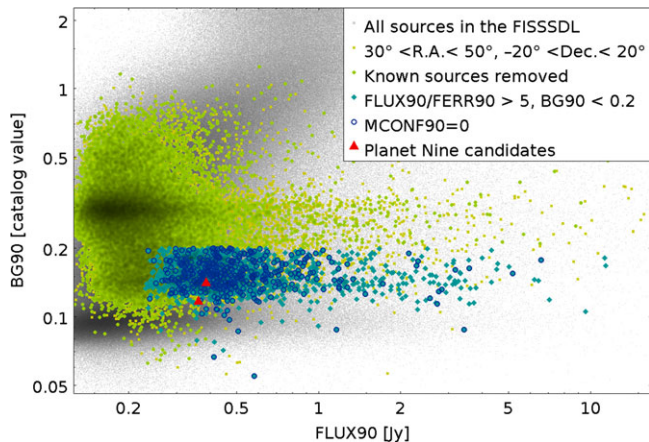


Figure 5. Candidates remained after each step on the 90 μm flux-background face value plot. All sources from FISSSDL are marked with grey dots. Sources in the region $30^\circ < \text{R.A.} < 50^\circ$, $-20^\circ < \text{Dec.} < 20^\circ$ are marked with yellow squares. Green circles are sources left after removing known sources by cross-matching with 9 catalogues (See Section 3.4). Light blue diamonds are $\text{FLUX90}/\text{FERR90} > 5$, $\text{BG90} < 0.2$ sources. The dark blue rings are sources with no monthly confirmation at 90 μm ($\text{MCONF90}=0$). Two Planet Nine candidates are shown in red triangles. The FLUX90 of these candidates are catalogue fluxes, so it is different from the per scan flux.

information on whether the source is detected at periods separated by six months (Monthly confirmation, $\text{MCONF90}=0$ when the source does not have monthly confirmation at 90 μm). We exclude sources confirmed over monthly intervals as they are not moving sources. We also remove sources only detected once in the 90 μm (WIDE-S) band. 393 candidates passed these selection criteria. All steps we performed before this section were based on the data in FISSSDL. The distribution of sources in the FLUX90 - BG90 plot is shown in Fig. 5.

3.7 Image inspection

We further examine the AKARI “detection probability maps” of 393 candidates. The detection probability map is an intermediate data for point source extraction, showing the likelihood of the presence of a point source at the sky position. It is an arbitrary unit, but in the FIS, source extraction >15 (catalogue unit) is adopted for the WIDE-S threshold for FISBSC. However, during the image inspection, we noticed detections with <21 are not reliable. Therefore, we only kept objects with >21 (catalogue unit) to guarantee effective detections. 24 out of 393 sources have the second detection with a likelihood between 15 and 21. We removed them since their second detections were not clear, and 369 candidates remained. Fig. 6 presents the detection probability map for one of the Planet Nine candidates. By analysing the timing of each scan, we can determine whether the candidate is a moving object. Specifically, we identify sources detected at least twice within 24 h, with no detections at the same location (within AKARI/WIDE-S’s beam size of $32''$, see Section 3.4) after six months. Out of 369

candidates, we selected 248 candidates that were clearly detected in all scans within 24 h. Out of 248 candidates, 83 uncertain sources without second detection images after a six-month separation period were excluded, as their movement could not be confirmed. Ultimately, we selected 165 candidates that were clearly detected in all scans within 24 h. They are confirmed to have no appearances before six months or disappear after six months.

During this process, we notice that around 50% of the ‘detections’ are CRs rather than true objects. Considerable CR hits create a special feature (see Fig. 7) and result in false detection when AKARI passed the South Atlantic Anomaly (SAA). These sources were rejected in the FISBSC confirmation process. Still, they remained in the FISSSDL because of relaxed conditions (FISBSC requires sources to be detected in at least 3/4 of the total number of scans observed at the position, which is not required for FISSSDL sources). After removing these sources, only 67 candidates are left.

Out of 67 candidates, 54 candidates’ detections are on the edge of the scan data, suggesting they might not be real detections. We removed these 54 candidates, and there are 13 candidates left. It is worth noting that there are 3 possibly fast-moving objects in our 13 Planet Nine candidates. They moved several arcminutes in a few hours, which is too fast to be Planet Nine but could be newly discovered asteroids. After removing these 3 fast-moving objects, we have 10 candidates.

The AKARI all-sky survey operation lasted about 16 months, so it is possible that AKARI scanned through the same position with a one-year time separation. In that case, the parallax vanishes, and the proper motion ranges from 1.2 to 6.4 arcmin. Only 8 out of 10 candidates have detection maps in the subsequent or the preceding year. Four of them have no nearby ($1.2' - 6.4'$) AKARI sources, so they are removed from the candidate list. Three of them only matched with monthly confirmed sources, so they were removed. One source has a matched source without monthly confirmation. However, that matched source was detected at the same epoch as our candidate; they are not Planet Nine. Ultimately, we have two Planet Nine candidates that were detected by AKARI in one epoch. Hereafter, we identify the candidates with their coordinates as FISSSDL Jxxxxxx±xxxxx and list them in Table 2.

A schematic selection process flow chart is shown in Fig. 8.

4. Final planet nine candidates

By identifying moving objects in AKARI FISSSDL and images, we found two Planet Nine candidates.

To analyse the physical properties of Planet Nine candidates, the fluxes of candidates are vital. However, the fluxes recorded in FISSSDL were not always the correct fluxes for these moving objects. In the standard procedure, the flux of a source is measured on the data constructed from all available scans. This process is designed for stable sources but will underestimate the fluxes of moving objects since they are not detected in all scans. We measure each scan’s flux of two candidates. The flux values for

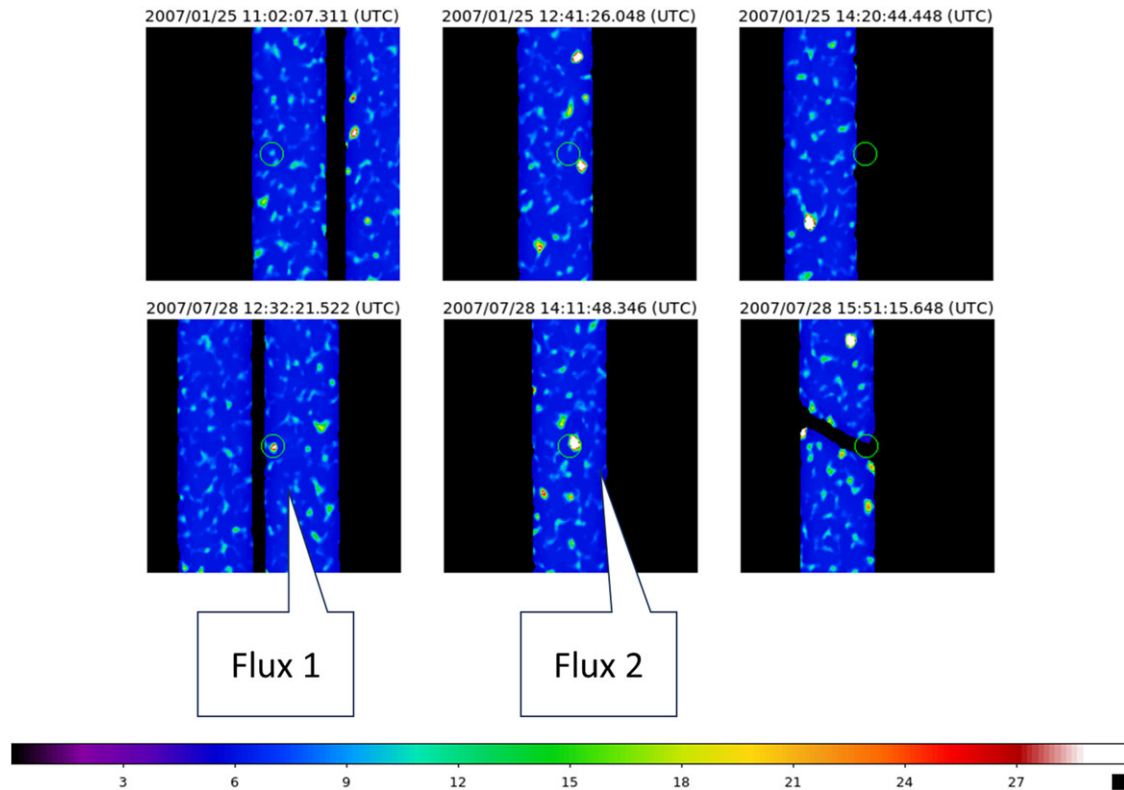


Figure 6. Each scan of FISSSDL J0250422-150114, one of the Planet Nine candidates. The image size is $30' \times 30'$, and the green circle is centred at the detection position with an $80''$ radius. The colour represents the likelihood of identifying a point source. The image value is in an arbitrary unit. In the point source extraction, pixels with ≥ 21 are treated as detections at the first step and sent to the confirmation process. FISSSDL J0250422-150114 was detected twice, which is labelled with Flux 1 and 2. The flux values are listed in Table 2.

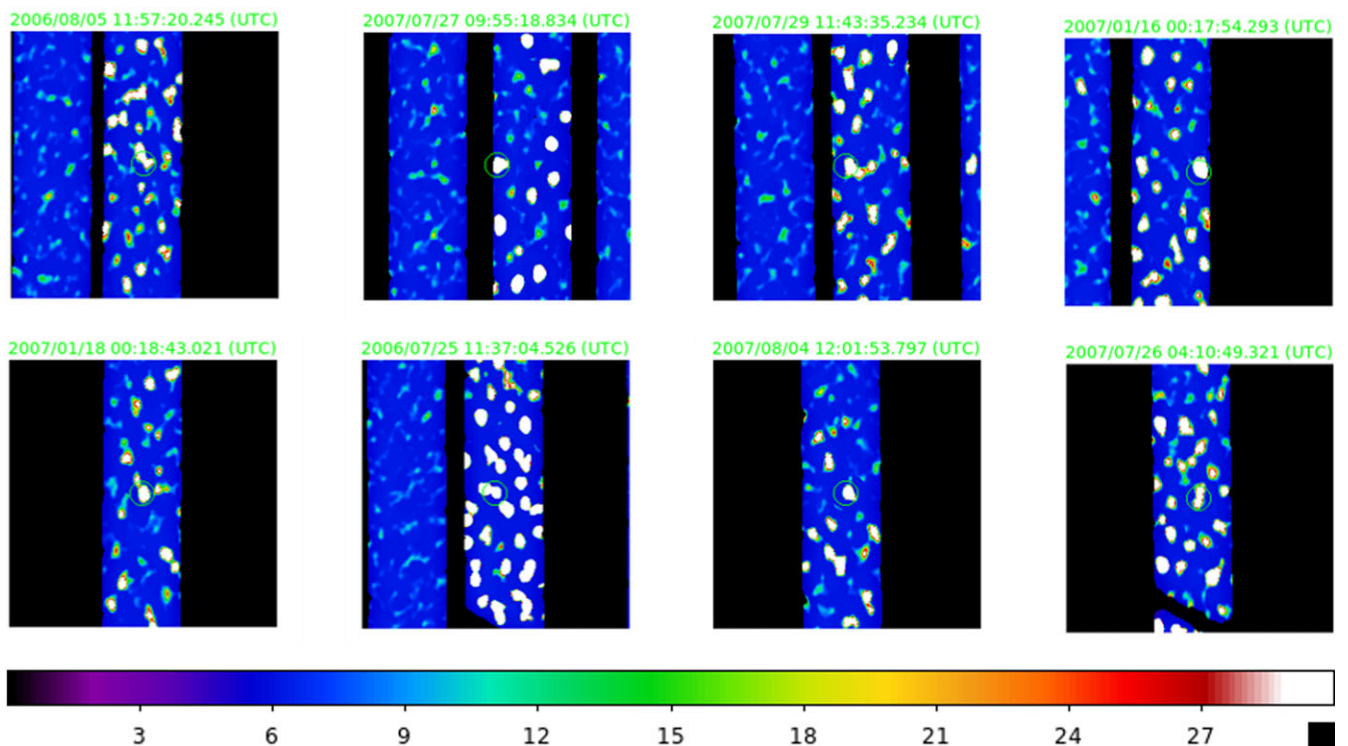


Figure 7. Fake detection caused by CRs when *AKARI* pass through SAA. These images are selected from different sources but with similar features. We reject the candidates contaminated by the CRs.

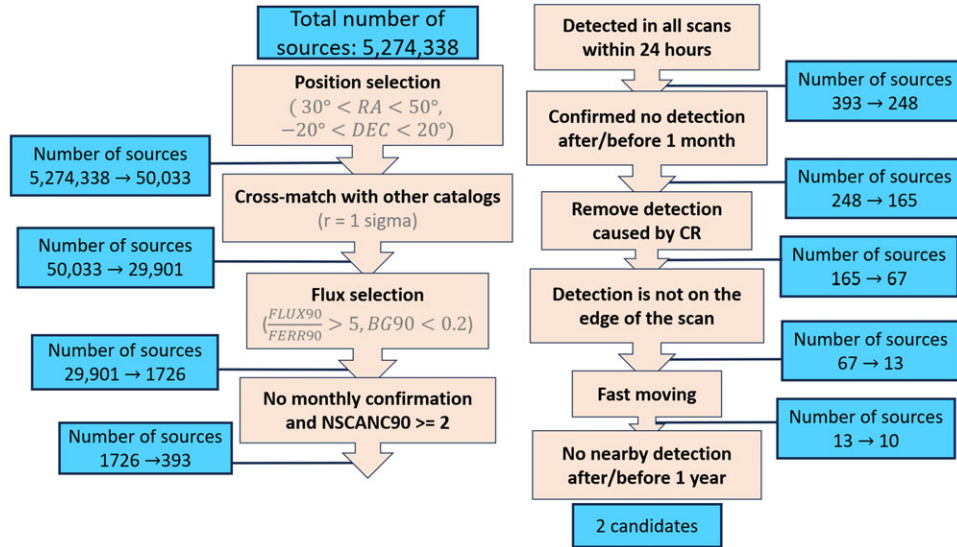


Figure 8. Work flow of this work. Orange blocks are steps we applied to select candidates. Blue blocks show the remaining sources after each step.

these candidates vary significantly in each scan, and we have only two detections. Therefore, we present their fluxes for each scan in Table 2.

During the *AKARI*'s all-sky survey, there is a chance that *AKARI* detected Planet Nine twice at different positions and times. These two detections might be included in our candidates as two separate candidates. Therefore, we try to find if any pairs of candidates fit the expected Planet Nine parallax among those 83 uncertain sources removed in Section 3.6 and the two final candidates. Unfortunately, the separations between each other were all larger than 22.9 arcmin, which is too large for Planet Nine's predicted parallax (see Fig. 3).

5. Discussion and conclusion

Compared to the combined ZTF (Brown & Batygin 2022), DES (Belyakov, Bernardinelli, & Brown 2022), and Pan-STARRS1 (Brown, Holman, & Batygin 2024) searches, we search for Planet Nine at a larger distance. The combined ZTF, DES, and Pan-STARRS1 survey exclude the situation V magnitude brighter than 21, which roughly corresponds to a distance of 500 au (see Figure 9 of Brown & Batygin 2019). Our search radius extended to ~ 800 au if Planet Nine is 53 K. Sedgwick & Serjeant (2022) also searched for Planet Nine in the *AKARI* catalogues. However, they required detections in *AKARI* FISBSC and IRAS all-sky search and covered the distance range from 700 to 8 000 au, which is very different from this work. Phan et al. (2025) conducted a Planet Nine search with a similar scheme to Sedgwick & Serjeant (2022), but with more strict criteria on the flux quality and covering a shorter distance range (500–700 au). The epochs of IRAS and *AKARI* are separated by 23 yr, and those two works aim to detect Planet Nine's orbital motion. In contrast, this work is designed to find moving objects that match Planet Nine's half-year parallax.

It is possible that we found a transient event in the *AKARI* image, rather than a moving object. Here, we estimate the expected events of four types of transient events with a timescale of less than 6 months. To pass our selection criteria and contaminate Planet Nine candidates, the transients need to be brighter than the *AKARI*/WIDE-S detection limit (0.2 Jy, Fig. 1) and be detected

twice within one day. The time window for detecting a transient in one year will be $(T - 1)/365$, where T is the typical timescale of the transient. We adopt the *Planck15* cosmology (Adam et al. 2016), i.e., Λ cold dark matter cosmology with $(\Omega_m, \Omega_\Lambda, \Omega_b, h) = (0.307, 0.693, 0.0486, 0.677)$ in the volume calculation. The survey volume (V) is $\frac{4}{3}\pi\Omega D^3$, where Ω is the solid angle and D is the maximum luminosity distance to detect a transient.

- For core-collapse supernova (CCSN), the event rate is $1.06 \times 10^{-4} \text{Mpc}^{-3} \text{yr}^{-1}$ (Taylor et al. 2014). By scaling from the assumed far-infrared flux of around 1 mJy at $z = 0.083$ (377 Mpc) (Perley et al. 2022), CCSNe need to be closer than $D = 27.6$ Mpc to have $\text{FLUX90} \geq 0.2$ Jy. The volume to the 27.6 Mpc within the survey area is $V = 1\,708 \text{Mpc}^3$. After applying the time window with $T = 30$ days (Perley et al. 2022), we expect only 0.014 CCSNe will be detected within the survey area by the *AKARI*.
- For Type Ia supernova (SN Ia), the event rate is $2.43 \times 10^{-5} \text{Mpc}^{-3} \text{yr}^{-1}$ (Frohmaier et al. 2019). We assume the far-infrared flux is around 10 mJy at 20.23 Mpc (Johansson, Amanullah, & Goobar 2013). The SNe Ia need to be closer than $D = 4.5$ Mpc to have $\text{FLUX90} \geq 0.2$ Jy, where the volume is $V = 7.5 \text{Mpc}^3$. After applying the time window with $T = 20$ days (Riess et al. 1999), the expected number of SN Ia detected by *AKARI* within the survey area is 1.5×10^{-5} .
- For Galactic nova, the Galactic nova rate is $\sim 30 \text{yr}^{-1}$ (Kawash et al. 2021). We assume the nova distribution follows the Milky Way stellar mass distribution (Kawash et al. 2021). The thin disk, thick disk, and stellar halo model are from Robin et al. (2003). The bulge/bar model is from Simion et al. (2017). The scale length of the thin and thick disks is 2.5 kpc. $D = 15$ kpc is set to be larger than the radius of the Milky Way. The volume to 15 kpc within the survey area is $V = 650 \text{kpc}^3$. Using this model, we scale the nova rate in the Milky Way to 30 novae per year. After integrating the survey volume, we found that there are only 0.001 novae per year in our survey volume.

Since the IR flux of a nova is uncertain, we calculate the expected number of novae in our survey volume. Even assuming *AKARI* can detect every nova in the Milky Way, the expected number of detected novae is 7.8×10^{-5} with a time window $T = 30$ days (Chomiuk, Metzger, & Shen 2021).

- For tidal disruption event (TDE), the event rate is $1.3 \times 10^{-7} \text{Mpc}^{-3} \text{yr}^{-1}$ (Masterson et al. 2024), much lower than that of CCSN. Considering TDE is generally fainter than CCSN, TDE events do not contribute to most transient detection.

In conclusion, only ~ 0.014 (mostly CCSNe) transient events within one year are expected to be detected by *AKARI* in our survey region.

The noise fluctuation could also contribute to fake sources. We assume FISSSDL sources that were detected only once are not real sources. Because Planet Nine selection criteria require at least two hourly detections, we estimate the chance of two bright ($\text{FLUX90}/\text{FERR90} > 5$ and $\text{BG90} < 0.2$) singly detected sources overlapping. There are 486 singly detected FISSSDL sources with $\text{FLUX90}/\text{FERR90} > 5$ and $\text{BG90} < 0.2$ in our survey area. The average number of *AKARI* scans of these singly detected sources (N_{scan}) is 5.3. The mean number of fake sources per scan (\bar{N}) is $486/N_{\text{scan}}$. The density of fake sources (ρ_f) is \bar{N}/A_S , where $A_S = 800 \text{ deg}^2$ is the survey area. The cross-match radius is $32''$ (Section 3.4), so the area of overlapping (A_O) is $\pi(32/3600)^2 \text{ deg}^2$. The expected number of overlapping fake sources of two scans will be $\bar{N}\rho_f A_O = 0.0025$. With N_{scan} scans, the expected fake is $\bar{N}\rho_f A_O \binom{N_{\text{scan}}}{2} = 0.029$, where $\binom{N_{\text{scan}}}{2} = \frac{N_{\text{scan}}!}{N_{\text{scan}}! \times (N_{\text{scan}} - 2)!}$ is the binomial coefficient.

We cross-matched the 3 fast-moving objects (see Section 3.7) with the Minor Planet Center database^b to check if they are known asteroids. All of these 3 fast-moving objects are not known asteroids. However, we found four fast-moving objects in the FISSSDL that are known asteroids. They are Ceres, Patientia, Liguria, and Antiope. They were not on the candidate list since their BG90 are all larger than 0.2.

We select two Planet Nine candidates by identifying moving objects from the *AKARI* FISSSDL. These two objects were detected twice within 24 h, and not detected after six months. However, since the fluxes of candidates are degenerated with many parameters, such as distance, mass, temperature, etc., the physical properties of these Planet Nine candidates are hard to constrain.

To confirm whether any of them is Planet Nine, we need to determine their orbits. However, most of them have only two *AKARI* detections, which are insufficient to decide on their orbit. Therefore, follow-up observations are needed. For example, future observations can be conducted using the Subaru telescope. Planet Nine's maximum expected angular motion from 2006 to 2024 is $117''$ at 300 au. Many studies have given different predictions by assuming different Planet Nine orbital parameters. Brown & Batygin (2019) estimated Planet Nine has a $16 \pm 5^\circ$ inclination angle while ML17 gave a 30° inclination angle. To be inclusive, we assume a circular orbit with a minimum radius (300 au) and calculate the maximum displacement. With an expected R-band magnitude < 26 (Brown & Batygin 2019), the brightness and

motion of Planet Nine are within the capabilities of the Subaru Hyper Suprime-Cam (HSC, Miyazaki et al. 2018) with a few pointings per target. The HSC on Subaru features a 1.5° diameter field of view and only needs 503 s of exposure time to reach $5\text{-}\sigma$ S/N of a 26 mag point source in r2-band.

The follow-up observation will be essential to verify the Planet Nine hypothesis. The confirmation of Planet Nine and its orbit might be able to explain the orbital clustering of KBOs, which helps us to have a deeper understanding of the solar system's history.

Acknowledgements. We would like to express our deepest appreciation to the anonymous referee for the comprehensive and thoughtful review of our manuscript. Their detailed examination and insightful suggestions have played a crucial role in refining our work, and the constructive feedback has greatly enhanced the overall quality and clarity of the paper. TG acknowledges the support of the National Science and Technology Council of Taiwan through grants 108-2628-M-007-004-MY3, 110-2112-M-005-013-MY3, 111-2112-M-007-021, 111-2123-M-001-008-, 112-2112-M-007-013, 112-2123-M-001-004-, 113-2112-M-007-006-, 113-2927-I-007-501-, and 113-2123-M-001-008-. TN acknowledges the support by JSPS KAKENHI Grant Numbers 23H05441 and 23K17695. TH acknowledges the support of the National Science and Technology Council of Taiwan through grants 110-2112-M-005-013-MY3, 113-2112-M-005-009-MY3, 110-2112-M-007-034-, and 113-2123-M-001-008-. SH acknowledges the support of the Australian Research Council (ARC) Centre of Excellence (CoE) for Gravitational Wave Discovery (OzGrav) project numbers CE170100004 and CE230100016, and the ARC CoE for All Sky Astrophysics in 3 Dimensions (ASTRO 3D) project number CE170100013. This research is based on observations with *AKARI*, a JAXA project with the participation of ESA. This research has made use of the CDS cross-match service, Strasbourg Astronomical Observatory, France. This research has made use of the SIMBAD database, operated at CDS, Strasbourg, France. This publication makes use of data products from the Wide-field Infrared Survey Explorer, which is a joint project of the University of California, Los Angeles, and the Jet Propulsion Laboratory/California Institute of Technology, funded by the National Aeronautics and Space Administration. This publication makes use of data products from the Two Micron All Sky Survey, which is a joint project of the University of Massachusetts and the Infrared Processing and Analysis Center/California Institute of Technology, funded by the National Aeronautics and Space Administration and the National Science Foundation. This research has made use of services provided by the International Astronomical Union's Minor Planet Center.

References

- Adam, R., et al. 2016, *A&A*, 596, A108. issn: 1432-0746. <https://doi.org/10.1051/0004-6361/201628897>.
- Ahumada, R., et al. 2020, *ApJS*, 249, 3. <https://doi.org/10.3847/1538-4365/ab929e>. arXiv: 1912.02905 [astro-ph.GA].
- Bannister, M. T., et al. 2016, *AJ*, 152, 70. <https://doi.org/10.3847/0004-6256/152/3/70>. arXiv: 1511.02895 [astro-ph.EP].
- Batygin, K., & Brown, M. E. 2016, *AJ*, 151, 22. <https://doi.org/10.3847/0004-6256/151/2/22>.
- Batygin, K., Morbidelli, A., Brown, M. E., & Nesvorný, D. 2024, *ApJL*, 966, L8. <https://doi.org/10.3847/2041-8213/ad3cd2>.
- Belyakov, M., Bernardinelli, P. H., & Brown, M. E. 2022, *AJ*, 163, 216. <https://doi.org/10.3847/1538-3881/ac5c56>.
- Bernardinelli, P. H., et al. 2020, *PSJ*, 1, 28. <https://doi.org/10.3847/PSJ/ab9d80>. arXiv: 2003.08901 [astro-ph.EP].
- Brown, M. E., & Batygin, K. 2019, *AJ*, 157, 62. <https://doi.org/10.3847/1538-3881/aaf051>.
- Brown, M. E., & Batygin, K. 2021, *AJ*, 162, 219. <https://doi.org/10.3847/1538-3881/ac2056>.
- Brown, M. E., & Batygin, K. 2022, *AJ*, 163, 102. <https://doi.org/10.3847/1538-3881/ac32dd>.

^b<https://www.minorplanetcenter.net/cgi-bin/checkmp.cgi>.

- Brown, M. E., Holman, M. J., & Batygin, K. 2024, arXiv: 2401.17977 [astro-ph.EP].
- Chambers, K. C., et al. 2016, <https://doi.org/10.48550/arXiv.1612.05560>.
- Chomiuk, L., Metzger, B. D., & Shen, K. J. 2021, *AnRvA&A*, 59, 391. <https://doi.org/10.1146/annurev-astro-112420-114502>. arXiv: 2011.08751 [astro-ph.HE].
- Cowan, N. B., Holder, G., & Kaib, N. A. 2016, *ApJL*, 822, L2. <https://doi.org/10.3847/2041-8205/822/1/L2>.
- Fortney, J. J., et al. 2016, *ApJ*, 824, L25. <https://doi.org/10.3847/2041-8205/824/2/L25>. arXiv: 1604.07424 [astro-ph.EP].
- Frohmaier, C., et al. 2019, *MNRAS*, 486, 2308. issn: 0035-8711. <https://doi.org/10.1093/mnras/stz807>.
- Johansson, J., Amanullah, R., & Goobar, A. 2013, *MNRAS*, 431, L43. issn: 1745-3925. <https://doi.org/10.1093/mnras/slt005>. eprint: https://academic.oup.com/mnras/articlepdf/431/1/L43/54661361/mnrasl_431_1_L43.pdf.
- Kawada, M., et al. 2007, *PASJ*, 59, S389. issn: 0004-6264. <https://doi.org/10.1093/pasj/59.sp2.S389>.
- Kawash, A., et al. 2021, *ApJ*, 922, 25. <https://doi.org/10.3847/1538-4357/ac1f1a>.
- Mainzer, A., et al. 2011, *ApJ*, 731, 53. <https://doi.org/10.1088/0004-637X/731/1/53>. arXiv: 1102.1996 [astro-ph.EP].
- Marocco, F., et al. 2021, *ApJS*, 253, 8. <https://doi.org/10.3847/1538-4365/abd805>.
- Masterson, M., et al. 2024, *ApJ*, 961, 211. <https://doi.org/10.3847/1538-4357/ad18bb>.
- Meisner, A. M., Bromley, B. C., Nugent, P. E., Schlegel, D. J., Kenyon, S. J., Schlafly, E. F., & Dawson, K. S. 2017, *AJ*, 153, 65. <https://doi.org/10.3847/1538-3881/153/2/65>. arXiv: 1611.00015 [astro-ph.EP].
- Millholland, S., & Laughlin, G. 2017, *AJ*, 153, 91. <https://doi.org/10.3847/1538-3881/153/3/91>.
- Miyazaki, S., et al. 2018, *PASJ*, 70, S1. <https://doi.org/10.1093/pasj/psx063>.
- Murakami, H., et al. 2007, *PASJ*, 59, S369. issn: 0004-6264. <https://doi.org/10.1093/pasj/59.sp2.S369>.
- Naess, S., et al. 2021, *ApJ*, 923, 224. <https://doi.org/10.3847/1538-4357/ac2307>. arXiv: 2104.10264 [astro-ph.EP].
- Napier, K. J., et al. 2021, *PSJ*, 2, 59. <https://doi.org/10.3847/PSJ/abe53e>. arXiv: 2102.05601 [astro-ph.EP].
- Onaka, T., et al. 2007, *PASJ*, 59, S401. issn: 0004-6264. <https://doi.org/10.1093/pasj/59.sp2.S401>.
- Perley, D. A., et al. 2022, *ApJ*, 927, 180. <https://doi.org/10.3847/1538-4357/ac478e>.
- Phan, T. L., et al. 2025, <https://doi.org/10.48550/arXiv.2504.17288>.
- Riess, A. G., et al. 1999, *AJ*, 117, 707. <https://doi.org/10.1086/300738>.
- Robin, A. C., Reylé, C., Derrière, S., & Picaud, S. 2003, *A&A*, 409, 523. <https://doi.org/10.1051/0004-6361:20031117>.
- Rowan-Robinson, M. 2021, *MNRAS*, 510, 3716. issn: 0035-8711. <https://doi.org/10.1093/mnras/stab3212>.
- Schlafly, E. F., Meisner, A. M., & Green, G. M. 2019, *ApJS*, 240, 30. <https://doi.org/10.3847/1538-4365/aafbea>.
- Scholtz, J., & Unwin, J. 2020, *PhRvL*, 125, 051103. <https://doi.org/10.1103/PhysRevLett.125.051103>.
- Sedgwick, C., & Serjeant, S. 2022, *MNRAS*, 515, 4828. issn: 0035-8711. <https://doi.org/10.1093/mnras/stac2044>.
- Shankman, C., et al. 2017, *AJ*, 154, 50. <https://doi.org/10.3847/1538-3881/aa7aed>. arXiv: 1706.05348 [astro-ph.EP].
- Sheppard, S. S., & Trujillo, C. 2016, *AJ*, 152, 221. <https://doi.org/10.3847/1538-3881/152/6/221>. arXiv: 1608.08772 [astro-ph.EP].
- Simion, I. T., Belokurov, V., Irwin, M., Koposov, S. E., Gonzalez-Fernandez, C., Robin, A. C., Shen, J., & Li, Z.-Y. 2017, *MNRAS*, 471, 4323. <https://doi.org/10.1093/mnras/stx1832>. arXiv: 1707.06660 [astro-ph.GA].
- Skrutskie, M. F., et al. 2006, *AJ*, 131, 1163. <https://doi.org/10.1086/498708>.
- Taylor, M., et al. 2014, *ApJ*, 792, 135. <https://doi.org/10.1088/0004-637X/792/2/135>.
- The Dark Energy Survey Collaboration. 2005, <https://doi.org/10.48550/arXiv.astro-ph/0510346>.
- Wenger, M., et al. 2000, *A&AS*, 143, 9. <https://doi.org/10.1051/aas:2000332>. arXiv: astro-ph/0002110 [astro-ph].
- Wright, E. L., et al. 2010, *AJ*, 140, 1868. <https://doi.org/10.1088/0004-6256/140/6/1868>. arXiv: 1008.0031 [astro-ph.IM].
- Wu, Y., & Lithwick, Y. 2013, *ApJ*, 772, 74. <https://doi.org/10.1088/0004-637X/772/1/74>. arXiv: 1210.7810 [astro-ph.EP].
- Zacharias, N., Monet, D. G., Levine, S. E., Urban, S. E., Gaume, R., & Wycoff, G. L. 2004, *American Astronomical Society Meeting Abstracts*, Vol. 205, 48.15. <https://ui.adsabs.harvard.edu/abs/2004AAS...205.4815Z>.